Three-dimensional coherent transfer function for reflection confocal microscopy in the presence of refractive-index mismatch

Min Gu and Daniel Day

Centre for Micro-Photonics, School of Biophysical Sciences and Electrical Engineering, Swinburne University of Technology, PO Box 218, Hawthorn, Victoria, 3122, Australia

Osamu Nakamura and Satoshi Kawata

Department of Applied Physics, Osaka University, Suita, Osaka 565, Japan

Received September 26, 2000; accepted January 31, 2001; revised manuscript received February 6, 2001

The three-dimensional (3-D) coherent transfer function for reflection confocal microscopy of high-numerical-aperture objectives is derived and calculated in the presence of refractive-index mismatch when a laser beam is focused into a medium of refractive index different from its immersion medium. This aberrated coherent transfer function is then used to estimate the readout efficiency of 3-D data bits recorded in a thick medium. It is shown that the readout efficiency of confocal microscopy for 3-D bit data storage is decreased with the focal depth of an objective in a recording medium. However, a high readout efficiency can be maintained if the tube length of a reading objective is linearly altered to compensate for the spherical aberration caused by the refractive-index mismatch.

OCIS codes: 180.1790, 110.4850, 180.6900, 180.5810.

1. INTRODUCTION

One of the methods for recording information into a volume material is based on two-photon excitation.[1–8] As a result of the cooperative two-photon absorption, a physical and chemical reaction occurs only within the focal region of a high-numerical-aperture objective. Consequently, information can be recorded as a three-dimensional (3-D) bit array within a thick recording medium. Depending on the physical and chemical reaction in a recording process, one can choose a fluorescence optical microscope[5,7–9] or a phase contrast optical microscope[1–4] to read out the recorded data bits. In the latter case, a reflection-mode confocal scanning microscope can be used for reading out the data bits caused by a change in refractive index under two-photon excitation,[2,10] provided that the passband of the 3-D coherent transfer function (CTF) for reflection confocal microscopy overlaps the support region of spatial frequencies of recorded 3-D data bits.

The use of reflection confocal microscopy in 3-D optical data storage allows one to perform recording and reading in the same optical system, which may be miniaturized by using fiber-optical components in practice. In addition, a reflection confocal microscope exhibits a strong optical sectioning effect,[11,12] which provides high axial resolution in the reading process.[11,12] If a pinhole of appropriate size is selected in the reading process, unwanted signals resulting from background scattering may be reduced.[11]

However, the performance of confocal microscopy is strongly degraded when a reading beam is focused deeply into a recording material that has a different refractive index from its immersion medium. The mismatch of the refractive indices results in spherical aberration depending on the focal depth of an objective[13–15] and thus reduces the illumination power in the focal region.[7,15] Further, the resultant distortion of the 3-D diffraction pattern of an objective in the focal region reduces the strength of the 3-D CTF; the deeper the focal depth within a thick material or sample is, the stronger the reduction of the strength of the 3-D CTF will be. Accordingly, the readout efficiency of confocal microscopy is decreased with the focal depth even if the passband of the 3-D CTF overlaps the support region of spatial frequencies of recorded data bits.

The aim of this paper is to investigate the dependence of the 3-D CTF on the focal depth of an objective within a thick sample and to estimate the readout efficiency of reflection confocal microscopy for 3-D bit data storage. In Section 2, the 3-D CTF for reflection confocal microscopy is derived in the presence of refractive index mismatch. The dependence of the 3-D aberrated CTF on the focal depth inside a thick sample is numerically revealed in Section 3. The compensation for the spherical aberration is also studied in terms of change in tube length of an objective. In Section 4, the readout efficiency of reflection confocal microscopy is defined and calculated in terms of the 3-D aberrated and compensated CTF. As a complete discussion, the 3-D CTF for transmission confocal microscopy and the 3-D optical transfer function (OTF) for an objective are given in Appendix A.

0740-3232/2001/082002-07$15.00

2. COHERENT TRANSFER FUNCTION IN THE PRESENCE OF REFRACTIVE INDEX MISMATCH

Let us first consider that an incident plane wave is focused by a high-numerical-aperture circular objective from a medium of refractive index n_1 into a thick medium or sample of refractive index n_2. The diffraction pattern of the objective in the focal region within the second medium is distorted compared with the diffraction-limited pattern by an objective in a uniform medium.[16] This distorted diffraction pattern of an objective can be expressed, under the scalar approximation, as[13–15]

$$h(r,z) = A\int_0^a P(\theta_1)(\tau_s + \tau_p\cos\theta_2)J_0(krn_1\sin\theta_1) \times \exp(i\Phi + ikzn_2\cos\theta_2)\sin\theta_1 \mathrm{d}\theta_1, \quad (1)$$

which is also called the 3-D amplitude point spread function for an objective. Here θ_1 and θ_2 are the angles of a ray of convergence in the first and second media, respectively, and are linked by Snell's law. $P(\theta_1)$ is the apodization function for a high-numerical-aperture objective.[17,18] The radial and axial coordinates r and z are defined with respect to the diffraction-limited focus that would occur if no second medium were presented. τ_s and τ_p, the Fresnel transmission coefficients for s and p polarization states at the interface between the first and second media,[17] are the function of angles θ_1 and θ_2. The function Φ in Eq. (1) is called the spherical aberration function caused by the mismatching of the refractive indices[13–15] and is given by

$$\Phi = -kd(n_1\cos\theta_1 - n_2\cos\theta_2), \quad (2)$$

where d represents the focal depth measured from the interface of the two media to the diffraction-limited focus.[13] It is clear that when $n_1 = n_2 = n$; i.e., when the refractive index of the first medium matches that of a second medium, we have $\Phi = 0$. Thus Eq. (1) reduces to the 3-D amplitude point spread function for an objective in a uniform medium.[16]

The 3-D CTF for an objective inside the second medium can be obtained by performing the 3-D Fourier transform of Eq. (1) with respect to r and z[18] and is given by

$$c(l,s) = P'(l)\left\{\frac{\delta[s - (1-l^2)^{1/2}]}{(1-l^2)^{1/2}}\right\}, \quad (3)$$

where

$$P'(l) = P(\theta_1)\frac{(\tau_s + \tau_p\cos\theta_2)\exp(i\Phi)\cos\theta_2}{\cos\theta_1}, \quad (4)$$

$$l = \sin\theta_2. \quad (5)$$

Here l and s are the radial and axial spatial frequencies, respectively, and have been normalized by n_2/λ.

Performing the 3-D autoconvolution of Eq. (3) gives rise to the 3-D CTF for reflection confocal microscopy consisting of a point detector.[12] It is, however, noted that Eq. (3)

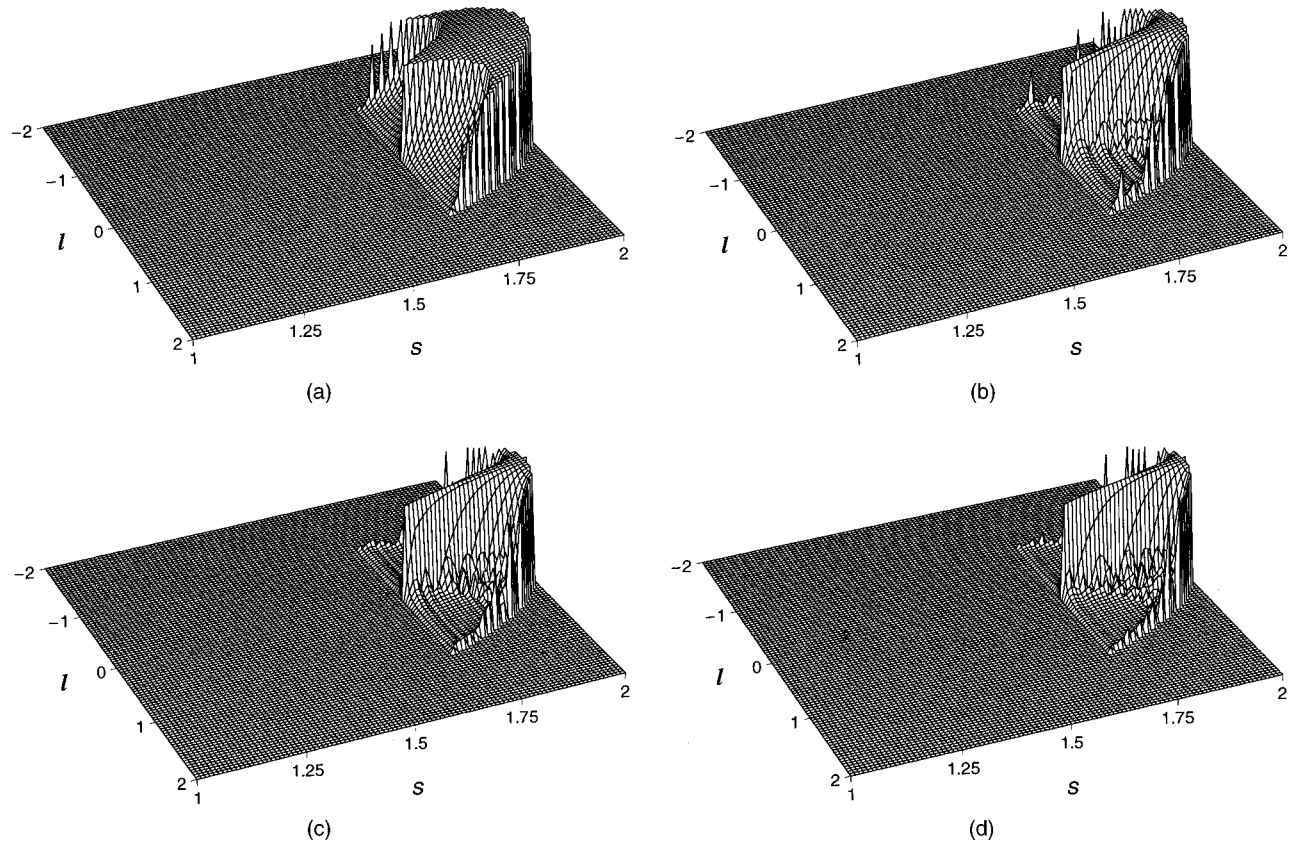

Fig. 1. Dependence of the modulus of the 3-D coherent transfer function on the focal depth d when a plane wave at wavelength 800 nm is focused by an objective (NA = 0.85) from air ($n_1 = 1$) to a medium of refractive index 1.59: (a) $d = 0$, (b) $d = 50\,\mu$m, (c) $d = 100\,\mu$m, (d) $d = 200\,\mu$m.

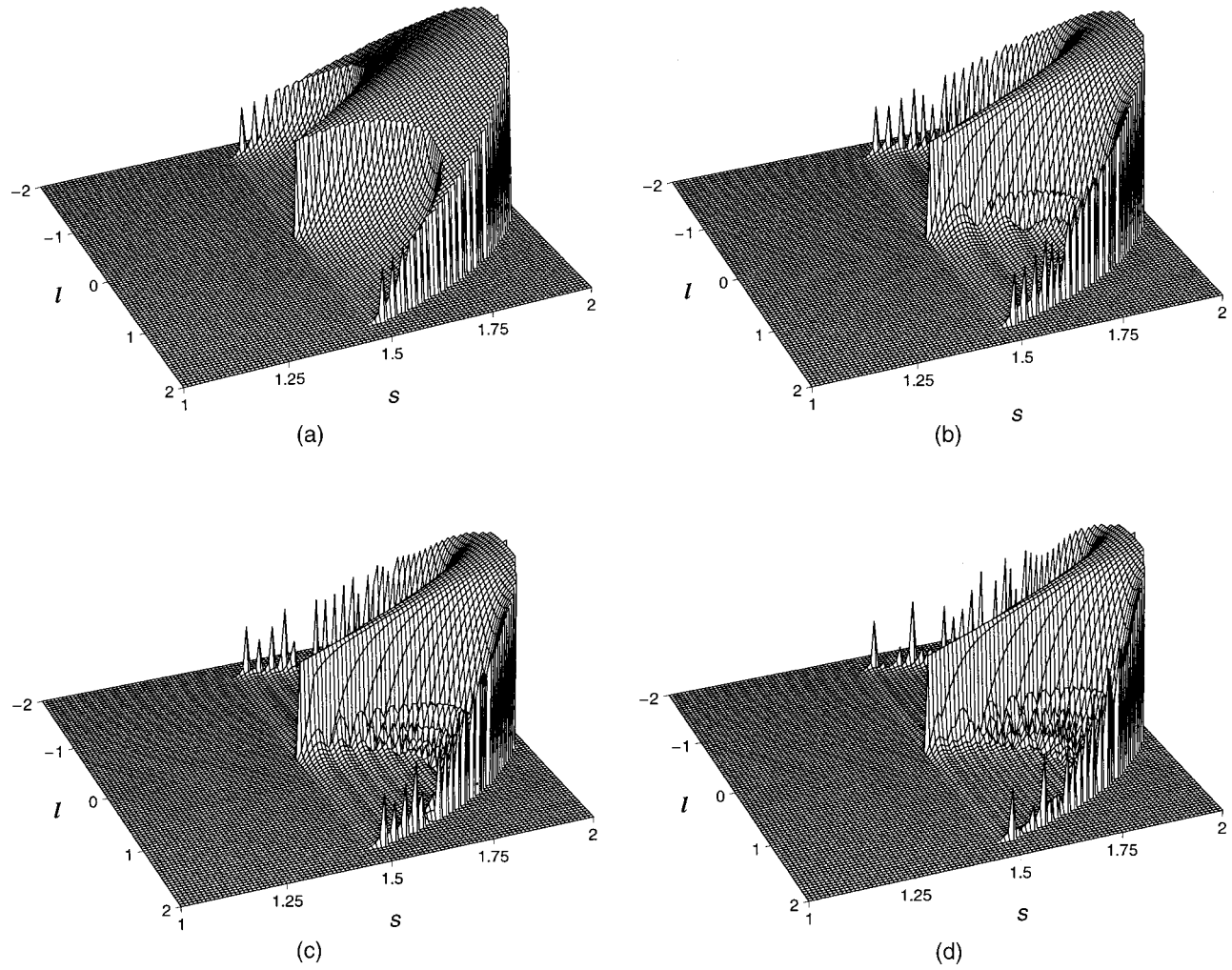

Fig. 2. Dependence of the modulus of the 3-D coherent transfer function on the focal depth d when a plane wave at wavelength 800 nm is focused by an objective (NA = 1.4) from immersion ($n_1 = 1.518$) to a medium of refractive index 1.59: (a) $d = 0$, (b) $d = 50\ \mu$m, (c) $d = 100\ \mu$m, (d) $d = 200\ \mu$m.

has the same form as the 3-D CTF for an objective in the absence of refractive-index mismatch[18] except for the replacement of $P(l)$ by $P'(l)$. Therefore the 3-D CTF for reflection confocal microscopy in the presence of refractive-index mismatch can be evaluated by the integral method reported elsewhere[19] (the 3-D CTF for transmission confocal microscopy in the presence of refractive-index mismatch is given in Appendix A):

$$c^r(l,s) = \frac{4}{\pi(l^2+s^2)^{1/2}} \begin{cases} \displaystyle\int_0^{\pi/2} P'(\theta_2^+)P'(\theta_2^-)\mathrm{d}\beta, & 2(l\sin\alpha + |s|\cos\alpha) \leqslant l^2+s^2 \leqslant 4 \\ \displaystyle\int_{\pi/2-\beta_0}^{\pi/2} P'(\theta_2^+)P'(\theta_2^-)\mathrm{d}\beta, & l^2+s^2 \leqslant 2(l\sin\theta + |s|\cos\alpha),\ |s| \geqslant 2\cos\alpha \\ 0, & \text{otherwise} \end{cases}. \quad (6)$$

Here

$$\beta_0 = \sin^{-1}\left[\frac{|s|(l^2+s^2)^{1/2}}{2l\left(1-\dfrac{l+s^2}{4}\right)^{1/2}}\left(1-\frac{2\cos\alpha}{|s|}\right)\right], \quad (7)$$

$$\cos\theta_2^{\pm} = \frac{|s|}{2}\left[1 \mp \cos\beta\frac{2l}{|s|(l^2+s^2)^{1/2}}\left(1-\frac{l^2+s^2}{4}\right)^{1/2}\right]. \quad (8)$$

The value of α is determined by

$$\alpha = \sin^{-1}\left(\frac{\mathrm{NA}}{n_2}\right), \quad (9)$$

where NA is the numerical aperture of the objective.

The passband of Eq. (6) has the same form as that in the absence of refractive-index mismatch but is defined within the second medium. It cuts off at $2\sin\alpha$ in the transverse direction, while it exhibits low and high cut-off

spatial frequencies at $2\cos\alpha$ and 2 in the axial direction. Unlike the aberration-free case,[19] the 3-D CTF in Eq. (6) becomes complex owing to the extra factor in Eq. (4). A complex CTF may alter image contrast at some spatial frequencies.

It should be pointed out that the 3-D CTF in Eq. (6) at $l = 0$ can be analytically expressed as

$$c^r(l = 0, s) = \frac{2\cos^2\theta_2}{|s|\cos\theta_1}(\tau_s + \tau_p\cos\theta_2)^2\exp(2i\Phi), \tag{10}$$

where $\cos\theta_2 = |s|/2$. It is therefore clear that the modulus of Eq. (10) is independent of the spherical aberration Φ, which is consistent with the conclusion based on the paraxial approximation.[20]

3. DEPENDENCE OF THE COHERENT TRANSFER FUNCTION ON THE FOCAL DEPTH

In all the numerical calculations, we assume that the objective obeys the sine condition, which leads to $P(\theta_1) = (\cos\theta_1)^{1/2}$, as shown in Refs. 16–18. Let us first consider a case of focusing a plane wave from air to a medium or sample of refractive index 1.59 (see Ref. 2). Figure 1 shows the corresponding 3-D CTF for reflection confocal microscopy at different focal depths. At the interface between the two media, the 3-D CTF is real and looks similar to that for the aberration-free case.[19] As soon as the focus of the objective is moved into the second medium or sample, the 3-D CTF becomes distorted. Like the 3-D aberrated CTF under the paraxial approximation,[20] there exist axial modulations in the 3-D CTF as shown in Fig. 1. At $d = 200\,\mu$m [Fig. 1(d)], the value of the 3-D CTF within its passband is almost zero except for the region near $l = 0$. This feature implies that only a thick object without transverse structures can be sharply imaged.

When an oil-immersion objective of numerical aperture 1.4 is used for imaging in reflection confocal microscopy, the passband of the 3-D CTF is significantly extended (see Fig. 2). The value of the 3-D CTF within the region of $2(l\sin\alpha + |s|\cos\alpha) \geqslant (l^2 + s^2)$ is modulated and reduced, but is not affected significantly in the region of $2(l\sin\alpha + |s|\cos\alpha) \leqslant (l^2 + s^2) \leqslant 4$. This property implies that if an oil-immersion objective of low numerical aperture is employed, the imaging performance of reflection confocal microscopy may not be degraded by the spherical aberration caused by refractive-index mismatch, as was observed in the experiment.[7]

There are a number of ways to reduce the effect of spherical aberration on 3-D imaging. One way is based on complex-pupil-function synthesis[21] and the other is based on change in tube length at which an objective is operated.[22] An alteration of tube length of a high-numerical-aperture objective results in primary spherical aberration given, under the sine condition, by[22]

$$\Phi_1 = B\sin^4(\theta_1/2). \tag{11}$$

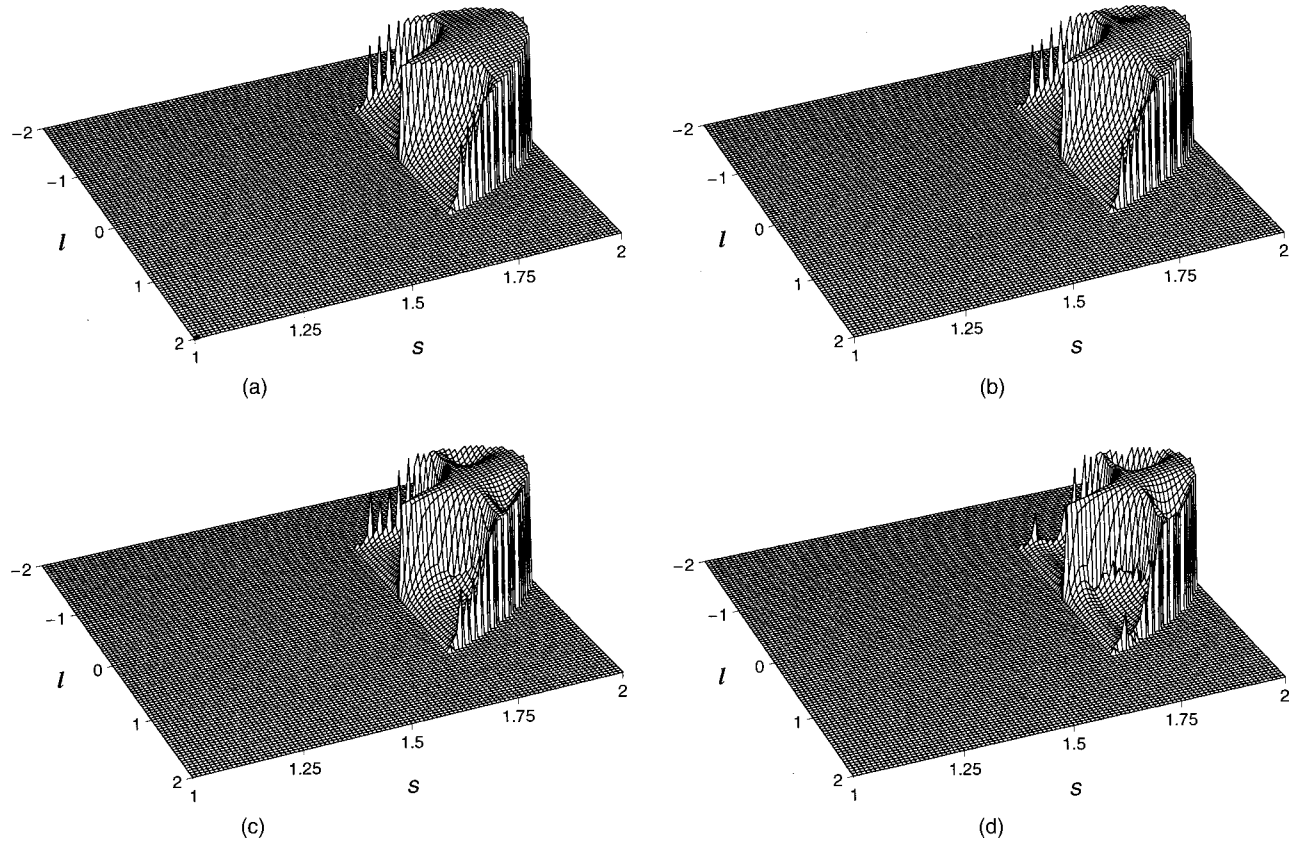

Fig. 3. Dependence of the modulus of the 3-D coherent transfer function on the focal depth d when a plane wave at wavelength 800 nm is focused by an objective (NA = 0.85) from air ($n_1 = 1$) to a medium of refractive index 1.59 under the compensation condition of $B = -1.5kd$: (a) $d = 50$, (b) $d = 100\,\mu$m, (c) $d = 200\,\mu$m, (d) $d = 400\,\mu$m.

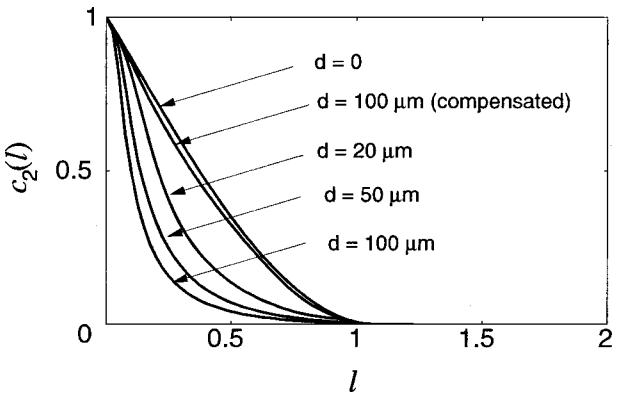

Fig. 4. Dependence of the modulus of the 2-D coherent transfer function for a dry objective of numerical aperture 0.85 on the focal depth ($d = 0$, 20, 50, and 100 μm).

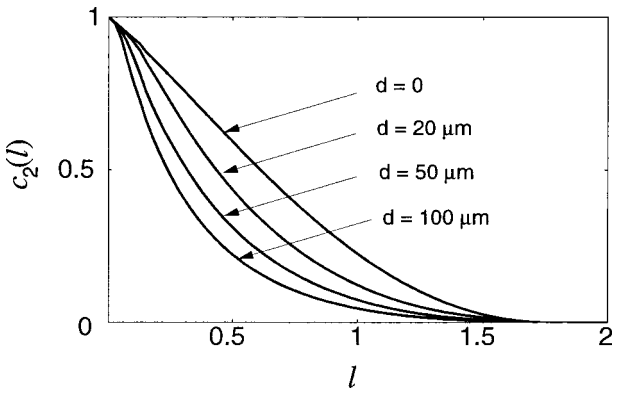

Fig. 5. Dependence of the modulus of the 2-D coherent transfer function for an oil objective of numerical aperture 1.4 on the focal depth ($d = 0$, 20, 50, and 100 μm).

The effect of the spherical aberration in Eq. (2) on the 3-D CTF can be compensated for by an alteration of tube length. It can be numerically shown that the 3-D amplitude point spread function in Eq. (1) is least affected by Eqs. (2) and (11) if

$$B \approx -1.5kd. \tag{12}$$

Under such a compensation condition, the 3-D CTF corresponding to Fig. 1 is displayed in Fig. 3. As expected, the 3-D CTF does not exhibit a pronounced reduction up to the focal depth at $d = 200\,\mu$m but shows modulations beyond that depth.

As a comparison, the modulus of the two-dimensional in-focus CTF for a thin structure embedded in a thick medium[23] $c_2(l)$, which is the projection of the 3-D CTF in the focal plane, is shown in Figs. 4 and 5. As expected, the two-dimensional CTF does not change significantly when the tube length of an objective is operated under the condition given by Eq. (12).

4. READOUT EFFICIENCY OF REFLECTION CONFOCAL MICROSCOPY

With the help of the 3-D CTF discussed in Sections 2 and 3, the measured image intensity of an object in a reflection confocal microscope can be expressed as[11,12]

$$I(x,y,z) = \left| \int_{-\infty}^{\infty} c(m,n,s)O(m,n,s) \times \exp[i2\pi(mx + ny + sz)]\mathrm{d}m\,\mathrm{d}n\,\mathrm{d}s \right|^2, \tag{13}$$

where $O(m,n,s)$ is the 3-D Fourier transform of an object function that is determined by the data bit array and gives the distribution of spatial frequencies in an object. It is clear that the right-hand size of Eq. (13) has a maximum value given by

$$I(x,y,z) \leqslant \int_{-\infty}^{\infty} |c(m,n,s)O(m,n,s)|^2 \mathrm{d}m\,\mathrm{d}n\,\mathrm{d}s. \tag{14}$$

In the case of two-photon excitation, the maximum signal in the reading process occurs when the passband of the 3-D CTF completely overlaps the support region of spatial frequencies of the recorded bits. Such a situation usually occurs when the material response under two-photon excitation becomes saturated if the peak power of a recording beam is too high. Thus the maximum readout signal is given by the total volume of the modulus of the 3-D CTF:

$$I(x,y,z) \leqslant M \int_{-\infty}^{\infty} |c(m,n,s)|^2 \mathrm{d}m\,\mathrm{d}n\,\mathrm{d}s. \tag{15}$$

Here M represents the maximum of the object spatial spectrum $|O(m,n,s)|^2$.

It is seen from Figs. 1–3 that the value of $\int_{-\infty}^{\infty}|c(m,n,s)|^2\mathrm{d}m\,\mathrm{d}n\,\mathrm{d}s$ reduces when the focal depth d of an objective becomes large. The value of $\int_{-\infty}^{\infty}|c(m,n,s)|^2\mathrm{d}m\,\mathrm{d}n\,\mathrm{d}s$ normalized by the value at $d = 0$ can be called the readout efficiency η.

For a reflection confocal microscope consisting of a circular objective, the readout efficiency corresponding to Figs. 1–3 is depicted in Fig. 6. It is noted that η decreases quickly when $d > 10\,\mu$m. Beyond this region, η exhibits an exponential decay with the focal depth d if there is no compensation by a change in tube length, and can be approximately expressed, for the cases in Figs. 1 and 2, as

$$\eta(d) \approx (1 - 0.35)\exp(-d/30) + 0.18, \qquad d > 20\,\mu\mathrm{m}, \tag{16}$$

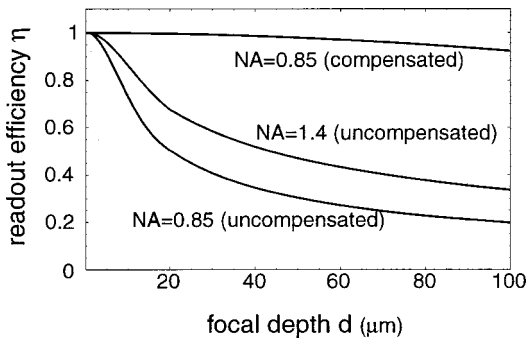

Fig. 6. Readout efficiency η of reflection confocal microscopy in 3-D data storage as a function of the focal depth d. The curve for NA = 1.4 (compensated) is similar to that for NA = 0.85 (compensated).

$$\eta(d) \approx (1 - 0.35)\exp(-d/39) + 0.29, \qquad d > 20\,\mu\text{m}, \tag{17}$$

respectively.

The readout efficiency exhibits an asymptotic value given by the volume of the modulus of the 3-D CTF near $l = 0$. This signal acts as a background in reflection confocal microscopy within a thick sample and should be avoided if high signal-to-noise ratio is needed. In that sense, 3-D bit data storage in a multilayered medium[23] leads to a high background, because the signal caused by the interfaces, imaged by the CTF $c(0, s)$, can be efficiently collected by a confocal microscope, resulting in a low signal-to-noise ratio. However, such a problem does not exist in 3-D bit data storage in a uniform thick medium.[2,4]

5. CONCLUSION

Under the scalar approximation, the 3-D CTF for reflection confocal microscopy of high-numerical-aperture objectives has been derived when a laser beam is focused into a thick sample that has a different refractive index from its immersion medium. The 3-D CTF in the presence of refractive-index mismatch is aberrated. The volume of the 3-D aberrated CTF is exponentially decreased with the focal depth of the objective in the thick sample. This feature leads to a reduction of the readout efficiency of reflection confocal microscopy in 3-D optical data storage. However, the effect of the spherical aberration can be compensated for by an alternation of tube length.

APPENDIX A

In the case of focusing a beam in a uniform medium, the 3-D CTF for transmission confocal microscopy is the same as the 3-D optical transfer function (OTF) for a high-numerical-aperture objective for incoherent imaging.[19] It is known from the transfer-function analysis under the paraxial approximation that the 3-D OTF for an objective is different from the 3-D CTF for transmission confocal microscopy if there is spherical aberration.[20] According to the integral method,[19] we can easily express the 3-D OTF for a high-numerical-aperture objective in the presence of refractive-index mismatch as

$$C(l, s) = \frac{4}{\pi(l^2 + s^2)^{1/2}} \begin{cases} \displaystyle\int_0^{\beta_0'} P'(\theta_2^+)P'^*(\theta_2^-)\mathrm{d}\beta, & l^2 + s^2 \leqslant 2(l\sin\alpha - |s|\cos\alpha) \\ 0, & \text{otherwise} \end{cases}, \tag{A1}$$

where P'^* represents the complex-conjugate operation of P',

$$\beta_0' = \cos^{-1}\left[\frac{|s|(l^2 + s^2)^{1/2}}{2l\left(1 - \dfrac{l^2 + s^2}{4}\right)^{1/2}}\left(\frac{2\cos\alpha}{|s|} + 1\right)\right], \tag{A2}$$

$$\cos\theta_2^{\pm} = \frac{|s|}{2}\left[\cos\beta\frac{2l}{|s|(l^2 + s^2)^{1/2}}\sqrt{1 - \frac{l^2 + s^2}{4}} \mp 1\right]. \tag{A3}$$

For transmission confocal microscopy, two objectives are involved in imaging.[11,12] A thick sample of refractive index n_2 is thus sandwiched within the medium of refractive index n_1. Assume that the thickness of the sample is L. Thus for a given focal depth of the first objective, the focal depth of the second objective is $L - d$. The spherical aberration presented to the first objective is given by Eq. (2), whereas the spherical aberration caused by the second objective is

$$\Phi'' = -k(L - d)(n_1\cos\theta_1 - n_2\cos\theta_2). \tag{A4}$$

Finally the 3-D CTF for transmission confocal microscopy becomes

$$c'(l, s) = \frac{4}{\pi(l^2 + s^2)^{1/2}} \begin{cases} \displaystyle\int_0^{\beta_0'} P'(\theta_2^+)P''(\theta_2^-)\mathrm{d}\beta, & l^2 + s^2 \leqslant 2(l\sin\alpha - |s|\cos\alpha) \\ 0, & \text{otherwise} \end{cases}, \tag{A5}$$

where

$$P'(\theta_2) = P(\theta_1)\frac{(\tau_s + \tau_p\cos\theta_2)\exp(i\Phi'')\cos\theta_2}{\cos\theta_1}. \tag{A6}$$

ACKNOWLEDGMENTS

The authors acknowledge support from the Australian Research Council. M. Gu thanks the Japan Society for Promotion of Sciences for the fellowship provided while he visited Osaka University.

Corresponding author Min Gu can be reached at the address on the title page or by e-mail at mgu@swin.edu.au.

REFERENCES

1. H. Strickler and W. W. Webb, "Three-dimensional optical data storage in refractive media by two-photon point excitation," Opt. Lett. **16**, 1780–1782 (1991).
2. A. Toriumi, S. Kawata, and M. Gu, "Reflection confocal microscope readout system in three-dimensional photochromic optical data storage," Opt. Lett. **23**, 1924–1926 (1998).
3. D. Day, M. Gu, and A. Smallridge, "Use of two-photon excitation for erasable/rewritable three-dimensional bit optical data storage in a photorefractive polymer," Opt. Lett. **24**, 948–950 (1999).
4. Y. Kawata, H. Ishitobi, and S. Kawata, "Use of two-photon absorption in a photorefractive crystal for three-dimensional optical memory," Opt. Lett. **23**, 756–758 (1998).
5. P. Cheng, J. Bhawalkar, S. Pan, J. Wiatakiewicz, J. Samarabandu, W. Liou, G. He, G. Ruland, N. Kumar, and P. Prasad, "Two-photon generated three-dimensional photon bleached patterns in polymer matrix," Scanning **18**, 129–131 (1996).
6. E. N. Glezer and E. Mazur, "Ultrafast-driven microexplosions in transparent materials," Appl. Phys. Lett. **71**, 882–884 (1997).
7. D. Day and M. Gu, "Effects of refractive-index mismatch on three-dimensional optical data storage density in a two-photon bleaching polymer," Appl. Opt. **37**, 6299–6304 (1998).
8. D. Ganic, X. Gan, and M. Gu, "Reduced effect of spherical aberration under two-photon excitation," Appl. Opt. **39**, 3943–3945 (2000).
9. M. Watanabe, S. Juodkazis, H. Sun, S. Matsuo, and H. Misawa, "Two-photon readout in three-dimensional memory in silica," Appl. Phys. Lett. **77**, 13–15 (2000).
10. M. Gu, "Conditions for confocal readout of three-dimensional photorefractive data bits," in *Photorefractive Optics: Materials, Properties and Applications*, F. T. S. Yu, ed. (Academic, London, 2000), pp. 307–331.
11. C. J. R. Sheppard, "Scanning optical microscopy," in *Optical and Electronic Microscopy* (Academic, London, 1987), pp. 1–98.
12. M. Gu, *Principles of Three-Dimensional Imaging in Confocal Microscopes* (World Scientific, Singapore, 1996).
13. P. Török, P. Verga, Z. Laczik, and G. R. Booker, "Electromagnetic diffraction of light focused through a planar interface between materials of mismatched refractive indices: an integral representation," J. Opt. Soc. Am. A **12**, 325–332 (1995).
14. P. Török, "Focusing of electromagnetic waves through dielectric interfaces—theory and correction of aberration," Opt. Mem. Neural Networks **8**, 9–24 (1999).
15. C. J. R. Sheppard and P. Török, "Effects of specimen refractive index on confocal imaging," J. Microsc. **185**, 366–374 (1997).
16. B. Richard and E. Wolf, "Electromagnetic diffraction in optical systems II: structure of the image field in an aplanatic system," Proc. R. Soc. London, Ser. A **253**, 358–379 (1959).
17. M. Born and E. Wolf, *Principles of Optics* (Pergamon, Oxford, UK, 1980).
18. M. Gu, *Advanced Optical Imaging Theory* (Springer–Verlag, Heidelberg, 1999).
19. C. J. R. Sheppard, M. Gu, Y. Kawata, and S. Kawata, "Three-dimensional transfer functions for high-aperture systems," J. Opt. Soc. Am. A **11**, 593–598 (1994).
20. M. Gu and C. J. R. Sheppard, "Effects of defocus and primary spherical aberration on three-dimensional coherent transfer functions in confocal microscopes," Appl. Opt. **31**, 2541–2549 (1992).
21. M. Neil, T. Wilson, and R. Juškaitis, "A wavefront generator for complex pupil function synthesis and point spread function engineering," J. Microsc. **197**, 219–223 (2000).
22. C. J. R. Sheppard and M. Gu, "Imaging by a high aperture optical system," J. Mod. Opt. **40**, 1631–1651 (1993).
23. M. Ishikawa, Y. Kawata, C. Egami, O. Sugihara, N. Okamota, M. Tsuchimori, and O. Watanabe, "Reflection-type confocal readout for multilayered optical memory," Opt. Lett. **23**, 1781–1783 (1998).